www.sciencemag.org/cgi/content/full/science.1256074/DC1

Supplementary Materials for

Intense foreshocks and a slow slip event preceded the 2014 Iquique M_w 8.1 earthquake

S. Ruiz,* M. Metois, A. Fuenzalida, J. Ruiz, F. Leyton, R. Grandin, C. Vigny, R. Madariaga, J. Campos

*Corresponding author. E-mail: sruiz@dgf.uchile.cl

Published 24 July 2014 on *Science* Express
DOI: 10.1126/science.1256074

This PDF file includes:

Materials and Methods

Relocations and moment tensor solutions

We located the precursory seismicity with the NonLinLoc software (*26*) using the velocity models proposed by *(27)*. We relocated 109 events with M_L larger than 4.0 in the period from 15 March to 1 April, using the CSN catalogue as reference.

Events with magnitude M > 4.6 were selected from the NEIC catalogue, because CSN only computes M_L for small events, and we inverted broadband records to retrieve moment tensor and the best centroid depth. The magnitude M_w that we computed may differ from that reported by the NEIC database, which is computed using teleseismic stations and usually provides mb for small magnitude events

GPS data processing

We used data from several cGPS networks spanning the entire South-American continent (Fig S10):

→ Specificaly **in Chile**, the LIA « Montessus de Ballore » Chilean-French network operated jointly by U-Chile, ENS, IPGP and IRD (50 stations): utar, mnmi, colc, psga, pcha, uape, hmbs, picc, mica, urcu, rado, pcal, pmej, ucnf, lvil, slmc, cnba, cmba, emat, pedr, pfrj, ovll, bton, tolo, junt, lsch, sill, crzl, vall, rcsd, dgf1, vnev, valn, robl, port, zapa, cern, lmel, navi, cabr, lemu, iloc, curi, maul, sjav, cons, pell, qlap, vita, plaj.

→ Stations from national networks in **Argentina, Bolivia and Brasil, and IGS stations** spanning the continent to constrain large scale deformation and define the reference frame.

- **IGS** (20 stations, available at all IGS data centers) : areq, braz, brft, kour, lpgs, sant, rio2, ispa, glps, cord, copo, conz, iqqe, lhcl, tucu, ufpr, chpi, cfag, antc, unsa.

- **RBMC** Brazil (14 stations) : cuib, maba, mscg, naus, poal, pove, savo, topl, mtvb, msdr, prcv, rocd, roji, rsal.

- **RAMSAC** Argentina (33 stations): abra, alum, azul, bcar, cata, csl0, csj1, dino, ebyp, esqu, jbal, ma01, meco, mzac, mzae, mzal, mzau, mzas, mzsr, nesa, ngaq, pejo, pdes, rwsn, sl01, srlp, tero, tilc, ucor, unro, unsj, vbca, ycba

- **IGM/DGFI** Bolivia (2 stations): scrz, urus

We processed all these data (119 stations) in 3 separate sub-networks : Central Chile, Northern Chile and large-scale South American plate, with enough redundancy (10 to 15 stations common stations) in order to combine them in a single solution later-on (Fig. S10). We reduced data in 24-Hour sessions to daily estimates of station positions using the GAMIT software, choosing the ionosphere-free combination, and fixing the ambiguities to integer values. We use precise orbits from the International GNSS Service for Geodynamics, precise EOPs from the IERS bulletin B, and IGS tables to describe the phase centers of the antennae. We estimate one tropospheric vertical delay parameter and two horizontal gradients per station every 3 h. The horizontal components of the calculated relative position vectors are precise to within a few millimeters for all pairs of stations, as measured by the root mean square (RMS) scatter about the mean (so-called baseline repeatability) or the high frequency scatter of the time series.

Reference frame realization and associated issues

We combine daily solutions using the GLOBK software in a "regional stabilization" approach. To define a consistent reference frame for all epochs (the ITRF2008 (28)), we use the stations from the different networks spanning the stable South American craton which have well determined positions and velocities in the ITRF2008 frame. We map our own daily realization into the reference frame by adjusting the coordinates of these stations to those defined in the ITRF in a least square iterative process. The post-fit residuals of these daily transformations range between

1 and 3 millimeter, depending on how many stations are actually available and the noise in their own time series with respect of their ITRF coordinates.

Most of the « stabilization » stations we used were located in Brazil, with the addition of Kourou in French Guyana and several sites in North-East Argentina. The stable Nazca plate is represented by only two available stations : ISPA and GLPS. This scheme produces daily time series from which we infer the transient signal during march 2014. We also generate weekly time series, reducing the high frequency noise by stabilizing the reference frame with a full week of data. However these series are not well suited for the analysis of a 3-week lasting transient.

After the 27 February 2010 Mw 8.8 Maule earthquake, many sites in the zone impacted by the earthquake show post-seismic relaxation. These sites cannot be used to define the stable South-American reference frame after 2010. Before 2010 we used 17 stations (BRAZ, KOUR, FORT, BRFT, PARA, ISPA, SAVO, TOPL, MSCG, CUIB, NAUS, POAL, CHPI, UFPR, SANT, LPGS, RIO2). After 2010 we had to remove SANT and LPGS. Several sites in Argentina and Chile also have velocities defined in the ITRF2008 but cannot be reliably used to define a stable reference frame for a long period of time since at one point or another they were affected by seismic events (eg COPO in 2006, IQQE in 2014, etc...).

Although they span the stable South American craton, and therefore show no tectonic motion other than the plate tectonic velocity itself, many stations located in Amazonia, Brasil show intense seasonal transients. NAUS (Manaus) or POVE (Porte Velho, located in a meander of the Madeira River) for example, show peak-to-peak variations of 8 (resp. 6) cm on the vertical component and 2 (resp. 1) cm on the Northern (resp. Eastern) component. These stations can still be used to define the long term reference frame (i.e. 10 years, the period of time over which seasonal effects almost average out), and allow us to determine very long term trends with

millimetric precision with respect to the stable interior of the plate. However, using them for the daily realization of the reference frame introduces a marked seasonal signal at all stations of the network. We therefore removed several of such stations (NAUS, POAL, and also CHPI, UFPR, CUIB) for our realization of the daily ITRF2008, which leaves us with 10 stations at least.

During a 2-year period (2011-2012), station GLPS was not operational, reducing the number of stations spanning the Nazca plate to only one (ISPA), which is the most important. Unfortunately, during the second semester of 2012, ISPA also stop providing data. During this 6 month period, the reference frame definition suffers from the lack of data at both stations. For this reason we refrain from commenting any transient signal in the network at this particular period of time.

Time-series analysis and SSE-related offsets

From the time-series ranging from 1 January 2012 to 1 April 2014, we simultaneously estimate : (1) a linear trend, to model the interseismic loading, (2) an annual periodic signal, to account for seasonal fluctuations in the time-series, (3) a step-function centered on 16 March 2014, to simulate the coseismic jump associated with the Mw 6.7 foreshock, and (4) a linear ramp function from 10 March to 1 April 2014, to constrain the signal induced by the SSE. Therefore, we can separate the coseismic motion of 16 March from the residual aseismic slip going on over the entire period, and very significant from 17 to 31 March at least. The choice of the inception time of the ramp-function, here chosen to be 10th of March to average the noise over the week preceeding the Mw 6.7 foreshock, only marginally affects the estimated cumulative displacement associated with the SSE.

We plot on Fig.3 of the main text the position of stations located along the coast for the 2014.0 to 2014.4 period in which the precursory motion developed, after subtraction of the interseismic and seasonal terms and removal of outliers after estimation of both white and flicker noise. Plots from January 2013 are shown in Figs. S11 and S12.

Overall, average weighted RMS of the residuals are 2.0 mm for both horizontal components, and 4.6 mm for the vertical component. Since station MNMI lacks data between 14 and 28 March, we are unable to separate the displacement associated with the SSE and the 16 March earthquake for this station (see Table S2).

SSE elastic modeling

We use the DEFNODE code developed by *(29*) to estimate the position and amplitude of the slip episodes associated with each phase of the precursory motion (i.e. coseismic motion associated to the Mw 6.7 earthquake, residual slow motion and cumulated motion over the sequence). The slab geometry has been considered as an homogeneously 20° dipping planar surface, similar to the one used to estimate the interseismic coupling coefficient *(5)*. We applied a 0.4m/° along-strike smoothing coefficient since it yields the best compromise between smoothing and RMS (i.e no significant improvement of the RMS is obtained using rougher solutions, see Fig S13) and forced the deeper nodes and lateral nodes to be fixed to limit edge effects. Our best-models are presented in Fig.4 of the main text.

As detailed in *(5)*, the shallowest part of the slab (z<15km) is unresolved using onland GPS measurements because the coast is located ~150 km away from the trench. Development of offshore geodesy is the only way to improve the resolution of both coseismic slip and interseismic coupling in this shallow part of the slab. We also refrain to interpret in too many details the along-dip variations of the slip since this is highly dependent on the slab geometry. Deep slip patches North and South of the bulk of slow slip are needed to improve the fit to UTAR and PB02 stations only, that remain however poorly fitted by our smooth model. Because of the large uncertainty on these measurements, we refrain to interpret these patches as slow-slip

occurring in the LCZs neighboring the Camarones segment. To conclude on this point, we should wait for other cGPS or campaign data to be available.

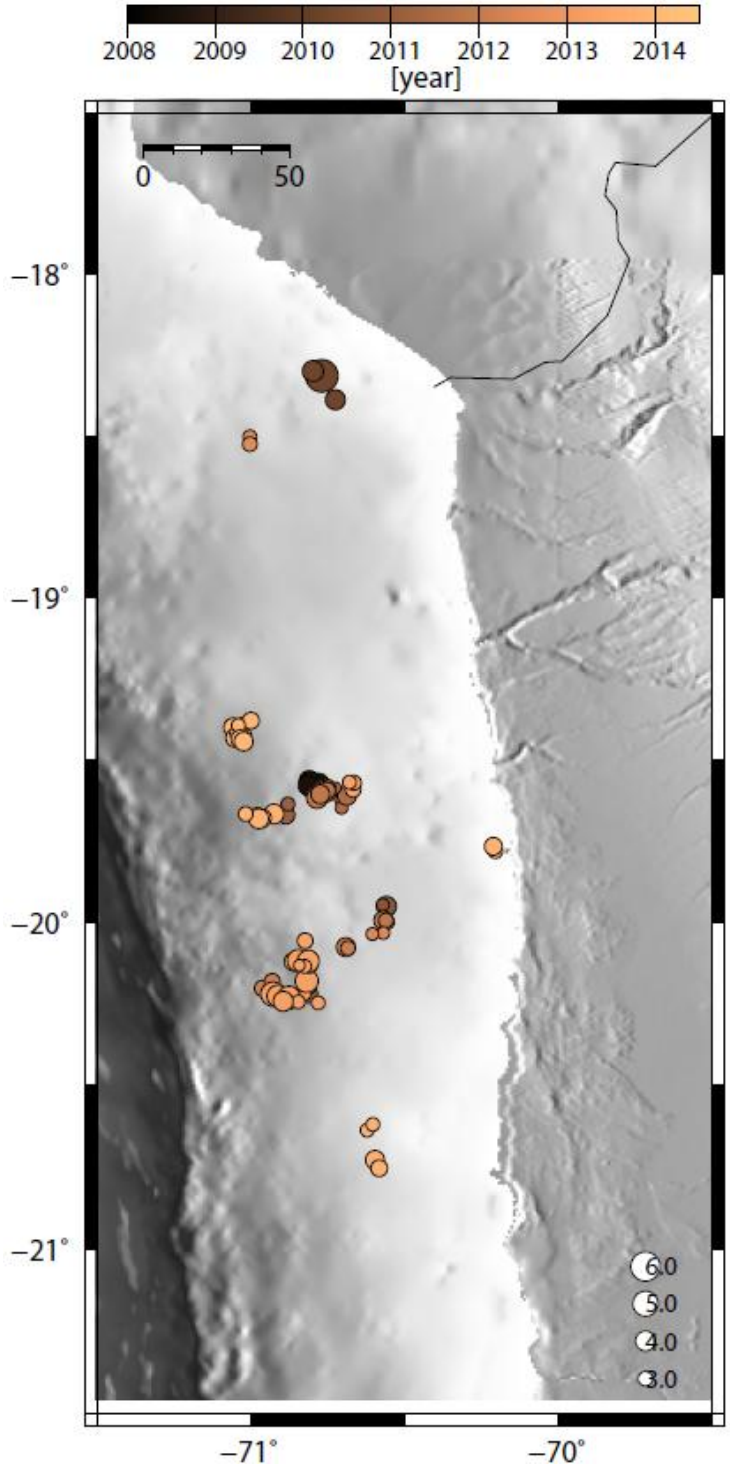

Figure S1. Identified clusters of the CSN catalogue shown in Fig. 1 and Table S1.

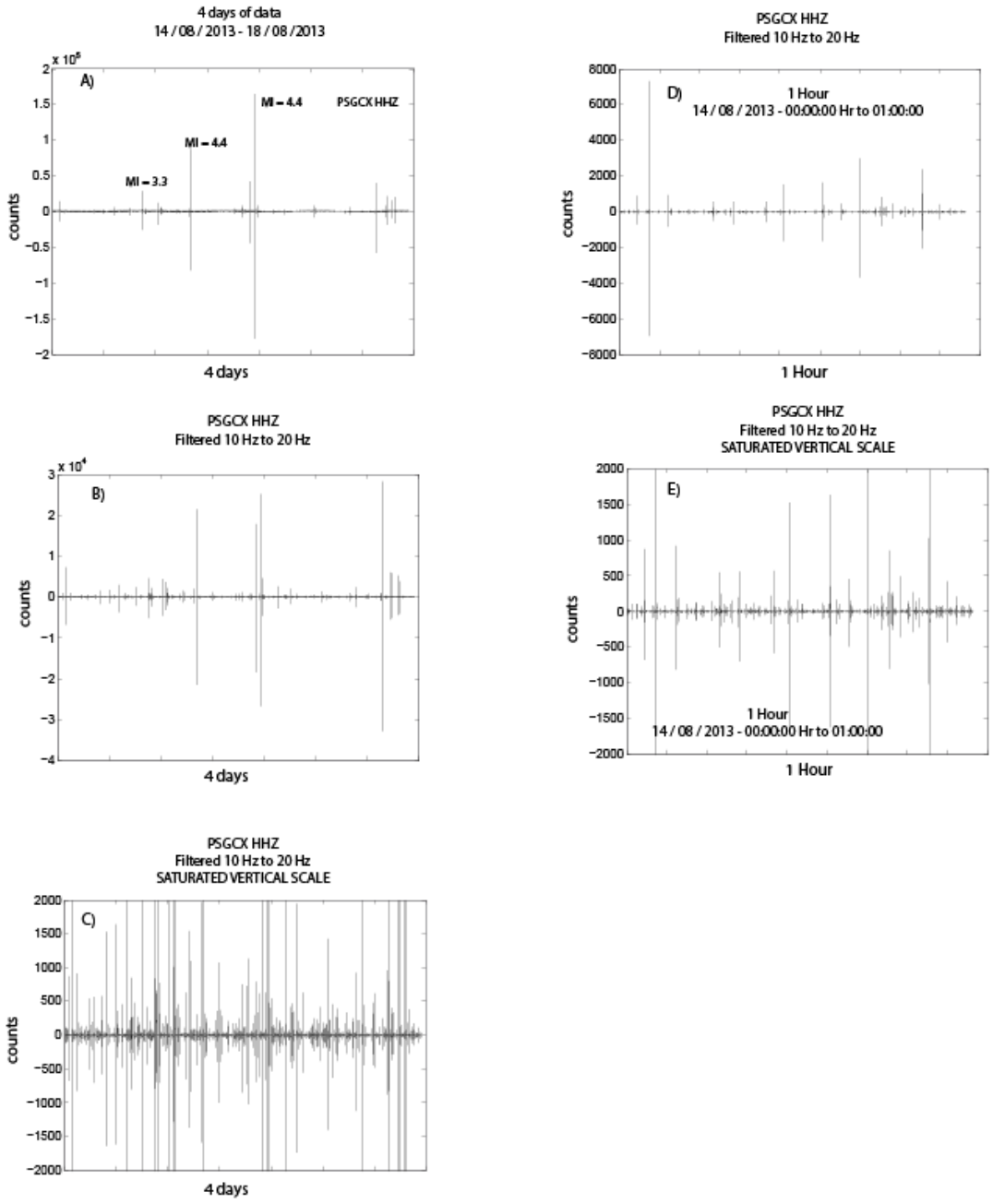

Figure S2. Record of almost continuous seismicity recorded near the Iquique earthquake in 2013. A) Seismic record of four days from 14 August to 18 August 2013 at the Pisagua (PSGCX) broad band vertical component. Ml indicates the local magnitude for three events located at ~20.1°S B) Previous record filtered between 10Hz to 20 Hz. C) Saturated vertical scale filtered

record. D) 1 Hour record from 00:00:00 to 01:00:00 of 14 August 2013. E) Saturated vertical scale of record shown in D).

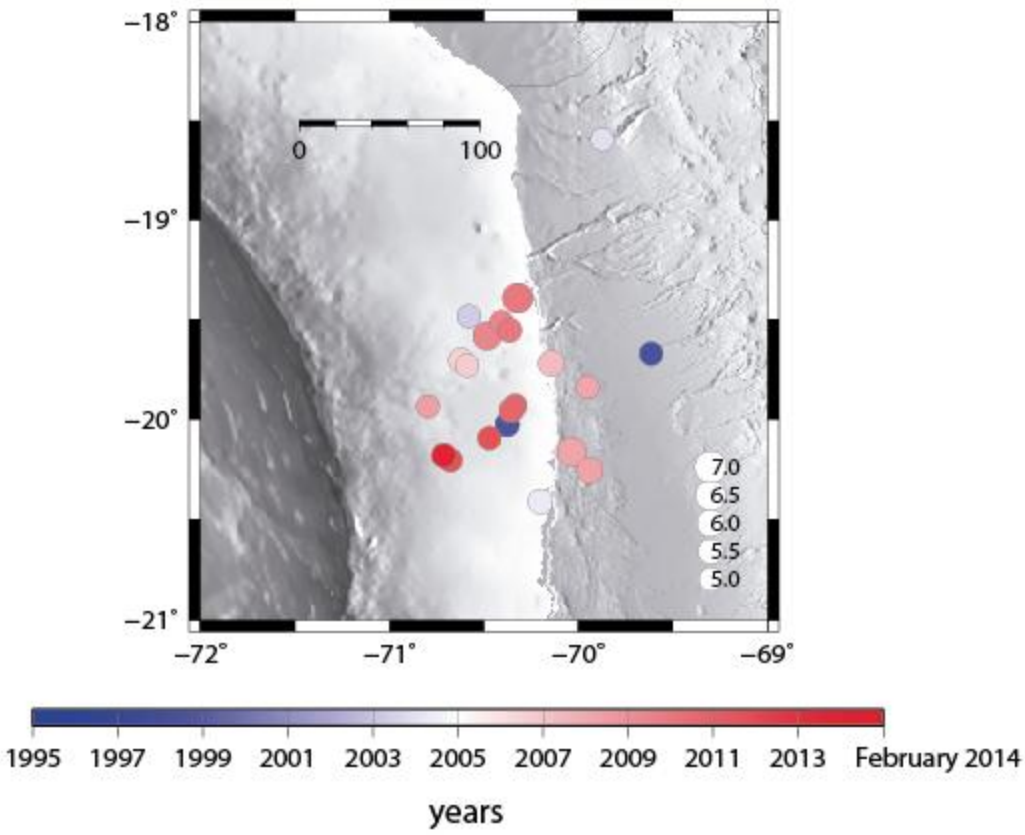

Figure S3. Events of magnitude larger than Mw 5.0 obtained from NEIC catalogue from 1995 to February 2014.

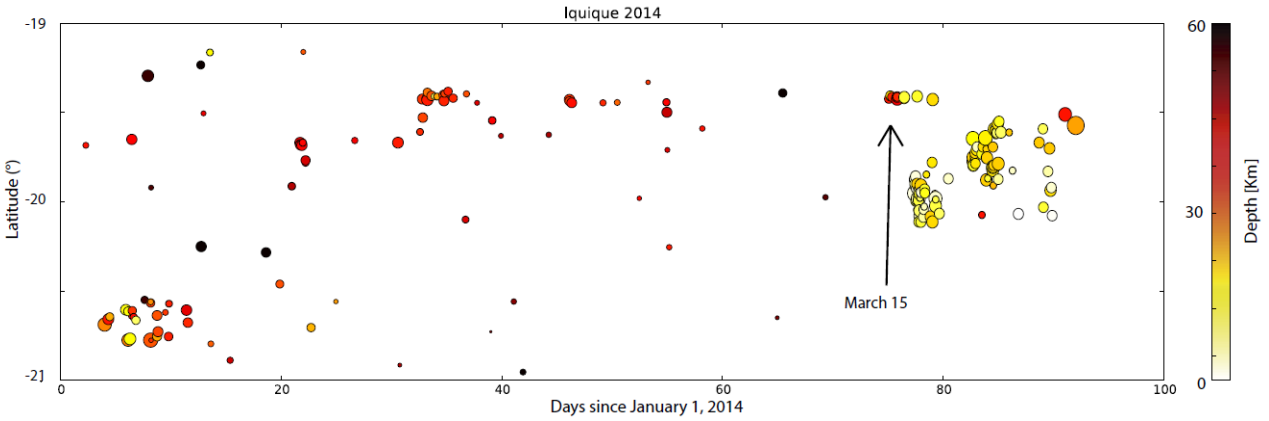

Fig. S4. Events located by CSN since January 1, 2014 to March 15, 2014. Our located events are shown since March 16.

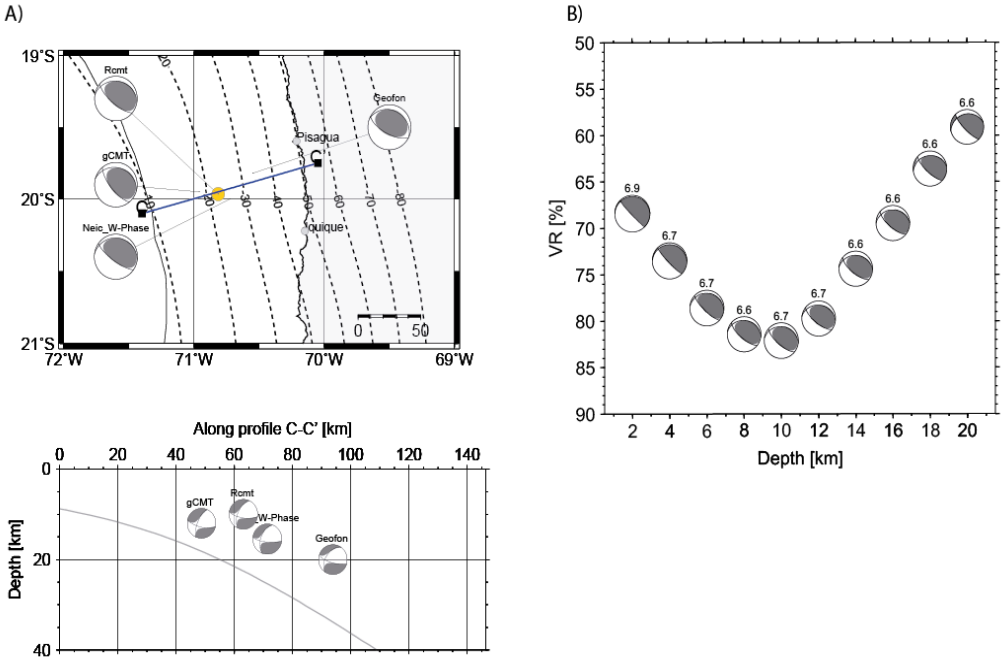

Fig. S5 Focal mechanism of the Mw 6.7, 14 March 2014 event. A) Comparison of centroid moment tensors reported by different agencies (gCMT, NEIC and Geofon) and the one proposed in this study (Rcmt). Map view and a cross-section C-C' are shown at the top and bottom, respectively. The Slab 1.0 model of the plate interface is shown by dashed and gray lines in each panel *(16)*. (b) Variance reduction as a function of source depth. Inverted regional moment tensor every 2 km depth is shown, as well as the moment magnitude above each focal sphere. The best moment tensor centroid is obtained for 10 km depth.

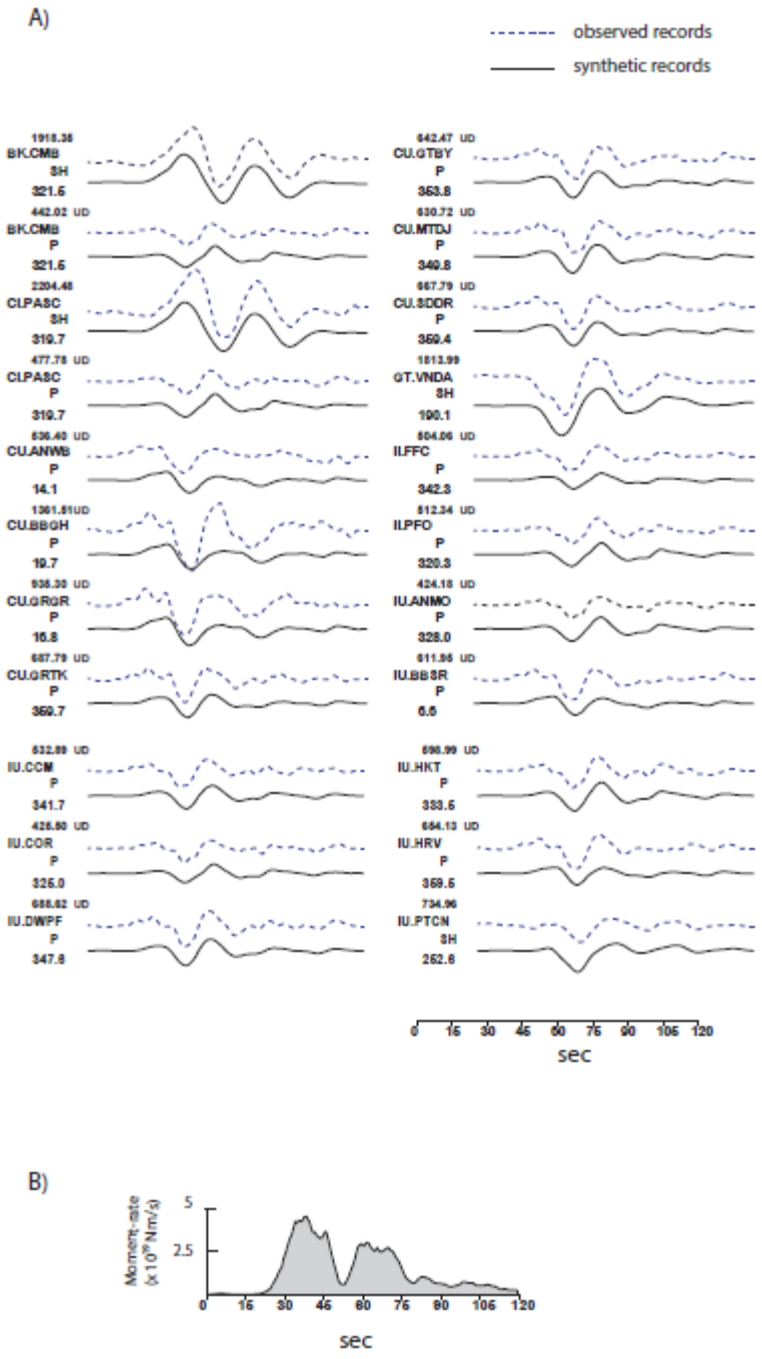

Fig. S6 A) Synthetic seismograms using Kikuchi Kanamori program *(17)* and observed far-field broad-band records of the FDSN network. B) Moment rate function of Iquique Mw 8.1.

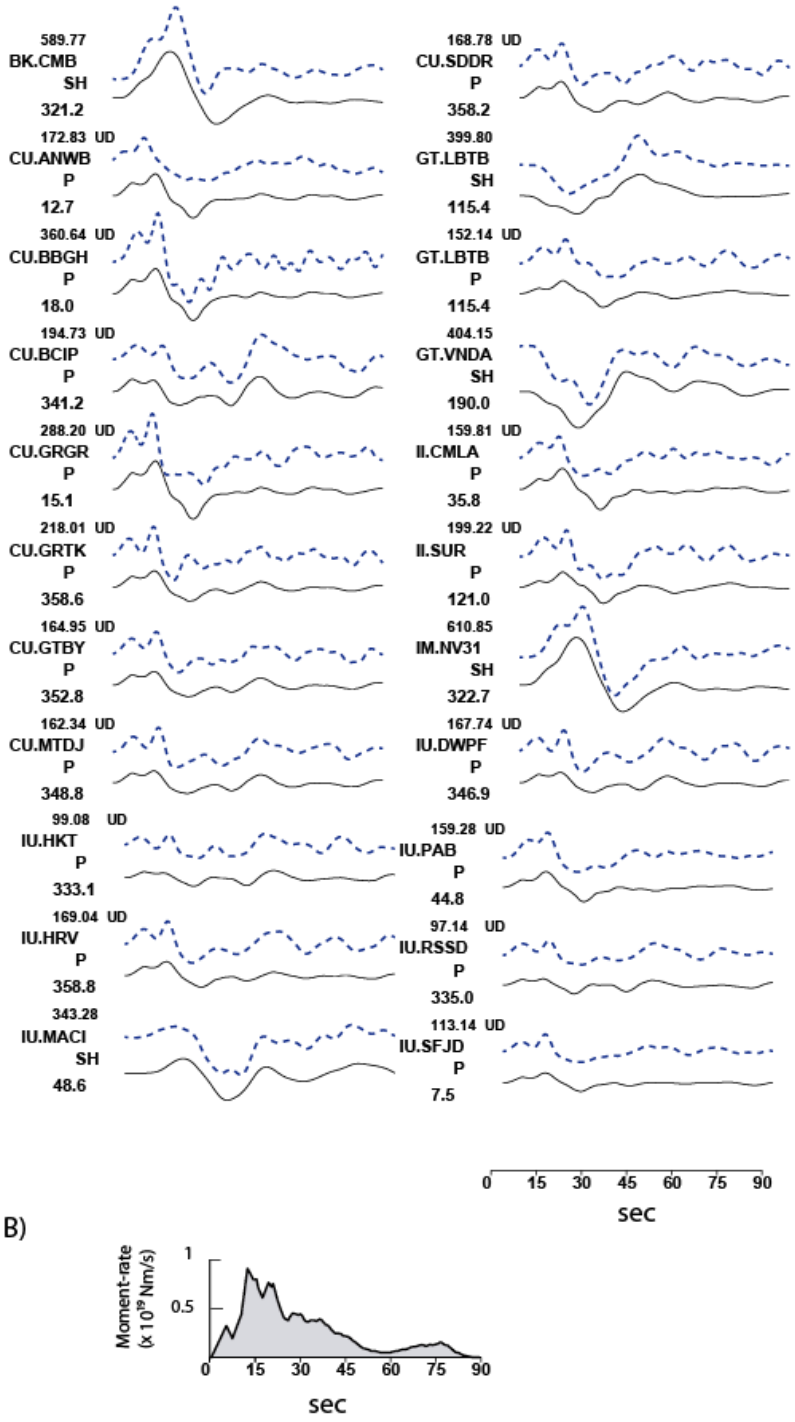

Fig. S7 A) Synthetic seismograms using Kikuchi Kanamori program *(17)* and observed far-field broad-band records of the FDSN network. B) Moment rate function of Iquique main aftershock Mw 7.6.

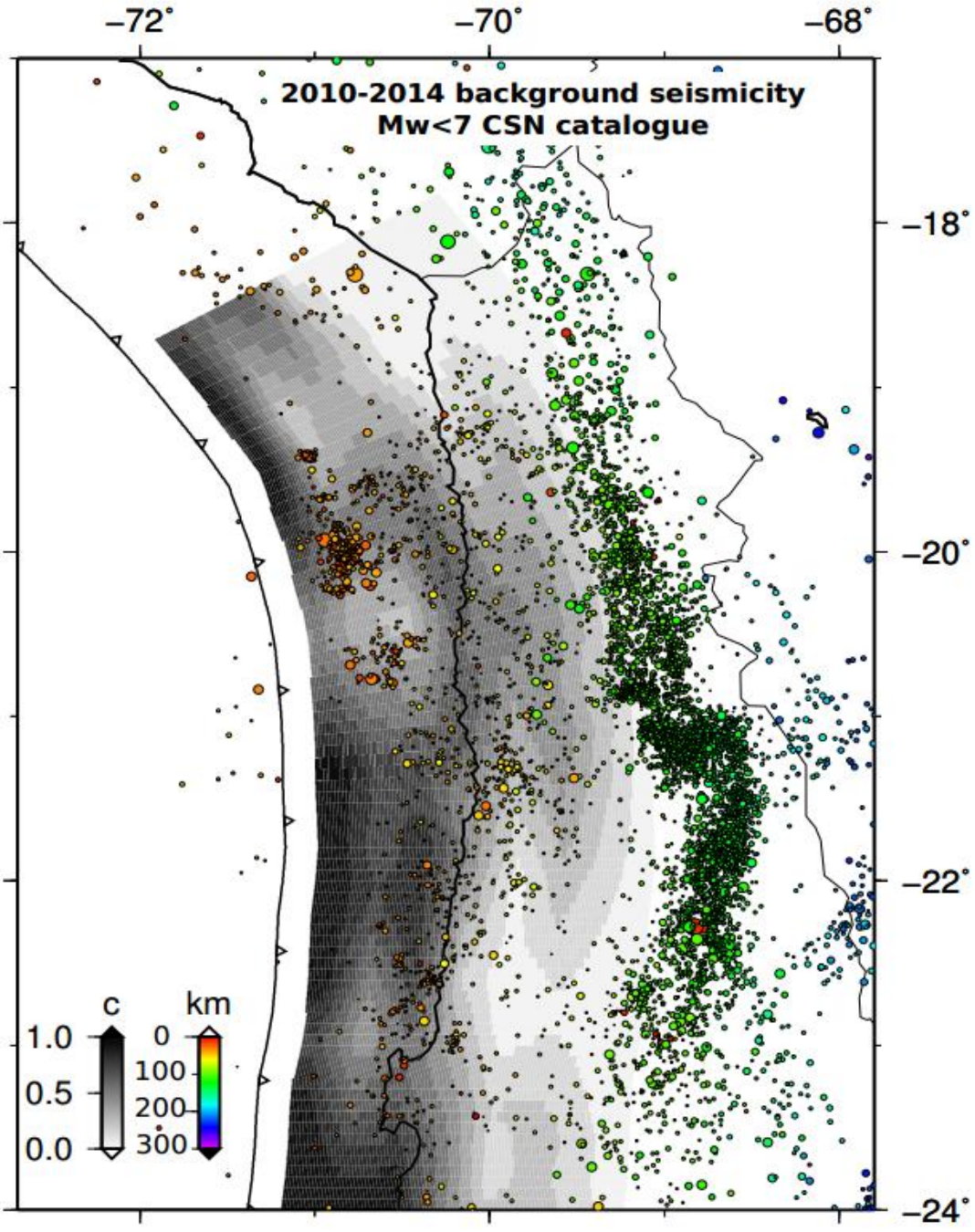

Fig. S8. Seismicity of CSN catalogue since 2010 to 2014 of magnitude smaller than Mw 7.0. The coupling is shown with grey color *(5)*.

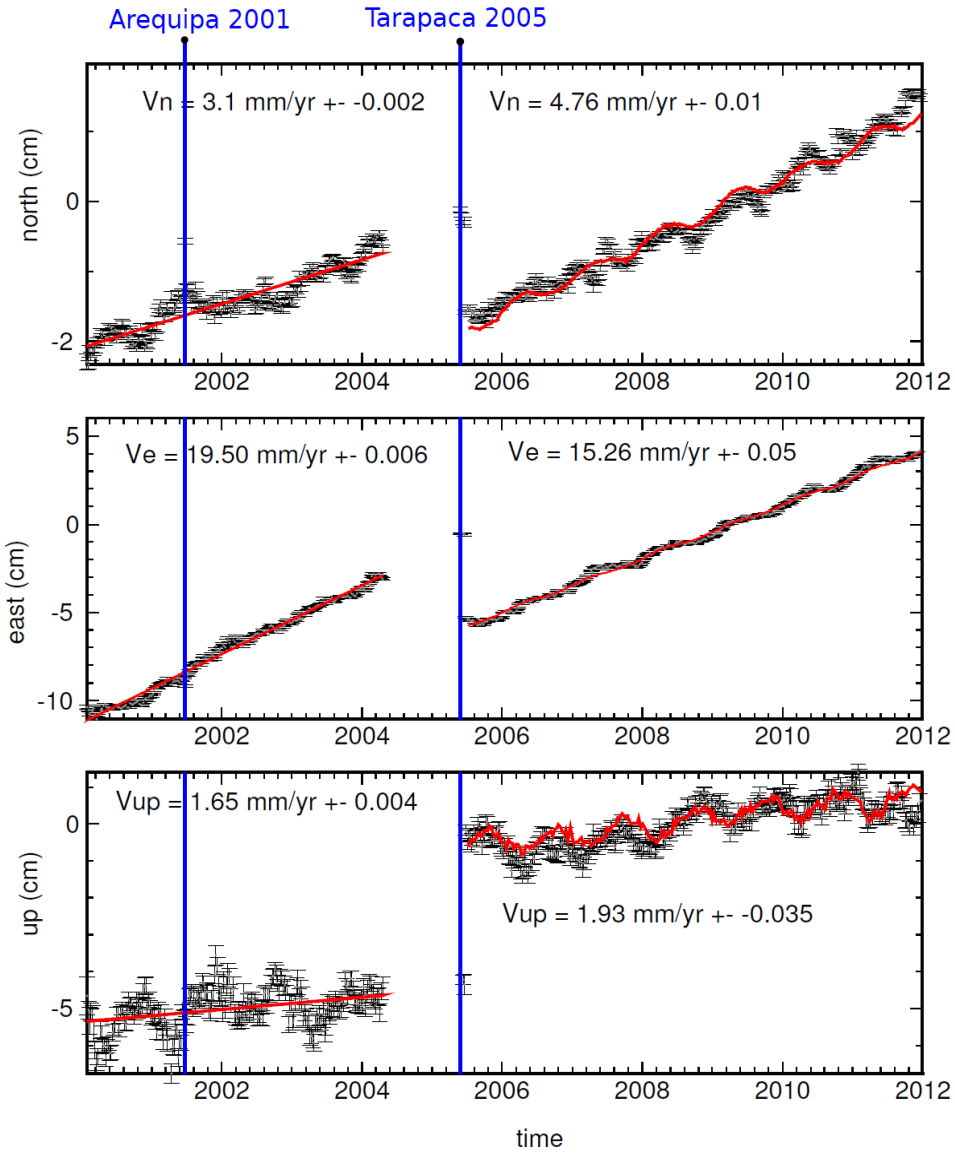

Fig. S9 : UAPE (Iquique center) time-series relative to stable South America (ITRF2008) processed using GAMIT-GLOBK . Coseismic offsets due to the 2001 Arequipa earthquake were corrected. The average velocity from 2001 to 2005 before the Tarapacà earthquake is indicated and plotted with red line. After 2005, the red curve stands for the averaged interseismic velocity corrected from the calculated elastic response to water loading based on Grace measurements (calculated following the methodology developed by *(30)).* A 4mm/yr decrease of the eastern interseismic loading rate is observed after 2005.

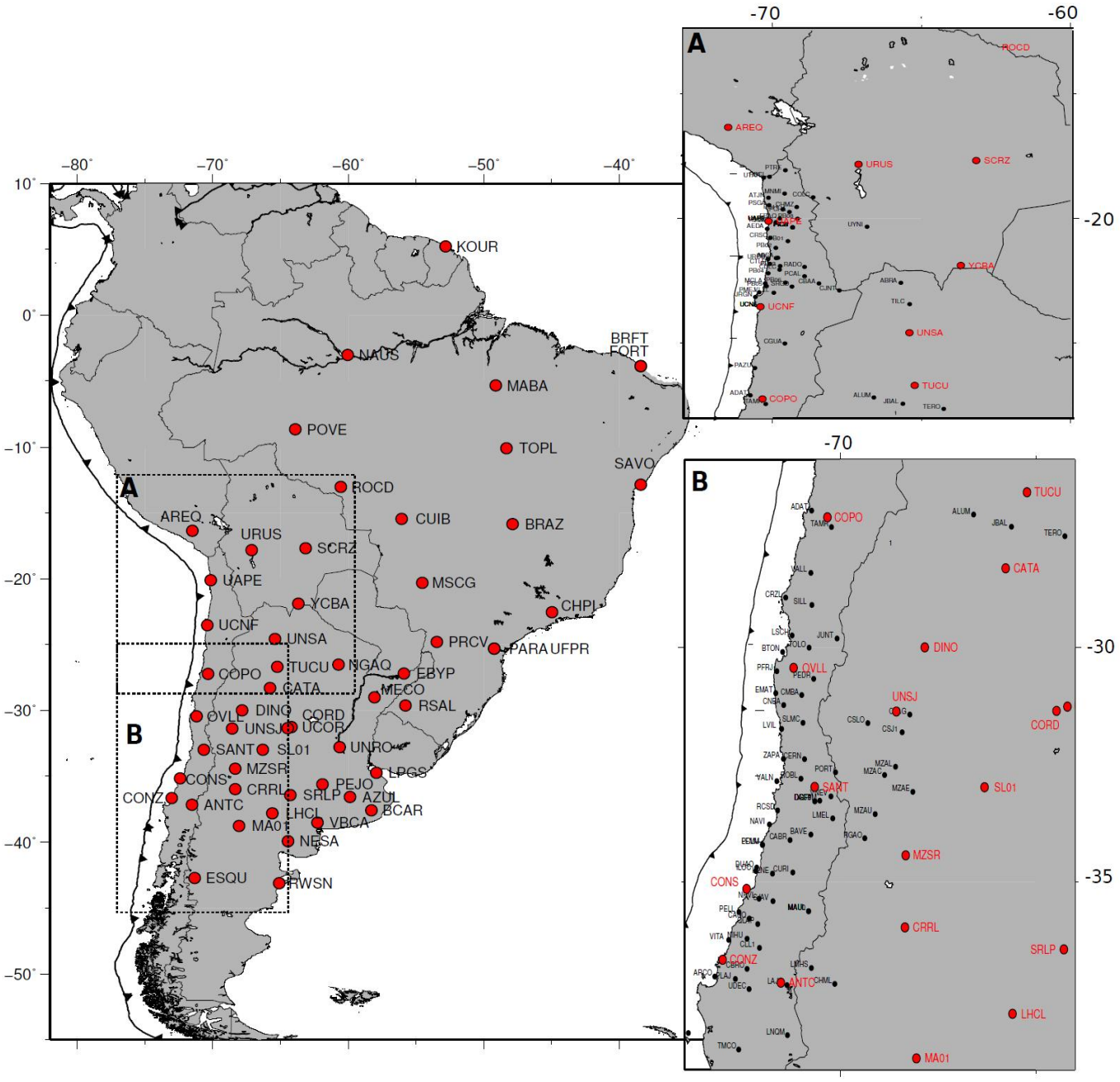

Fig. S10 : Maps of the 3 sub-networks processed separately and in combination. Red dots depict the stations of the large scale network (left frame) that are also processed with the more regional networks (A- north Chile; B- central Chile) to allow recombination of the whole.

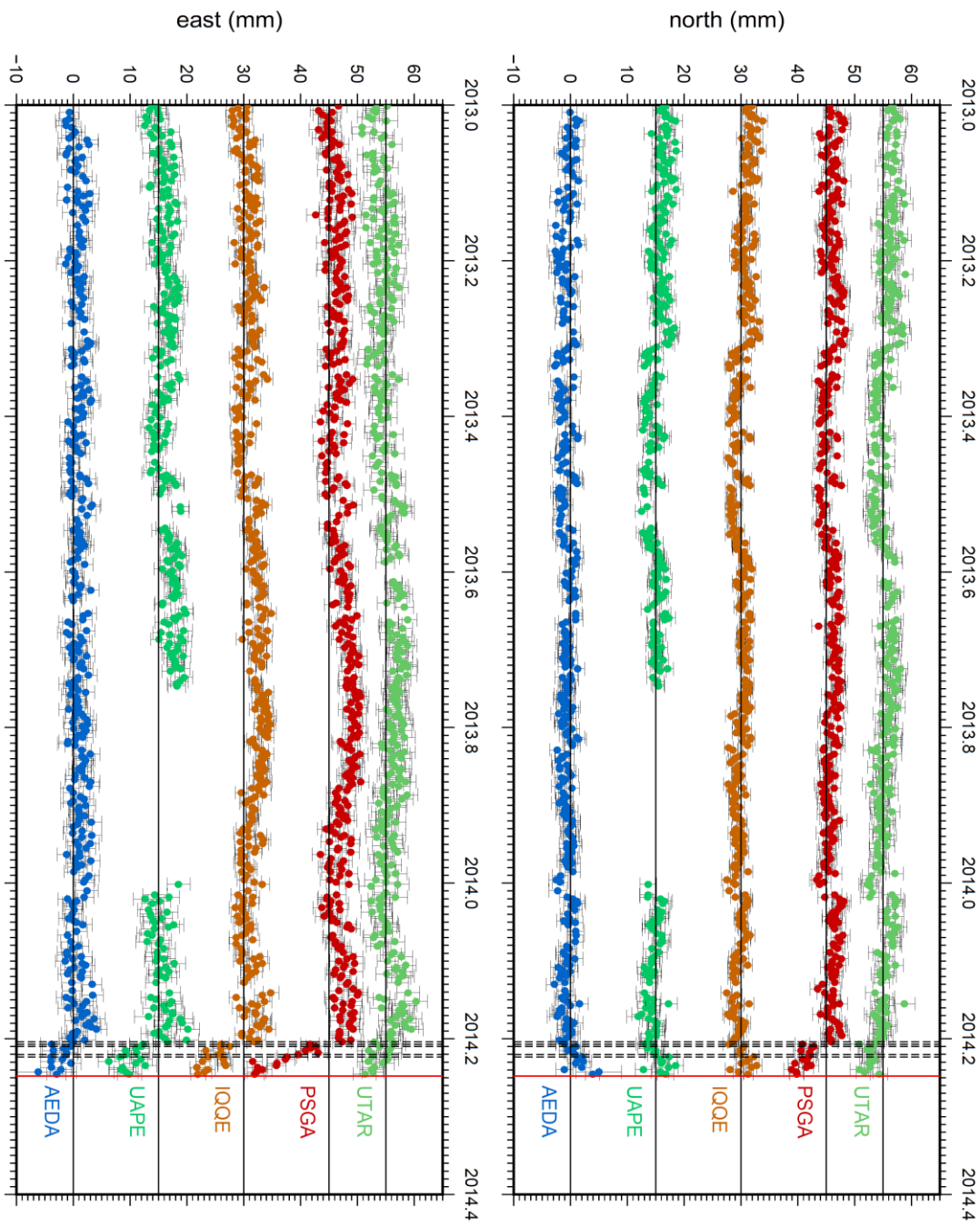

Fig. S11: Same as Fig.3 in the main text but presenting 2013-2014.4 time-series of closest GPS permanent stations.

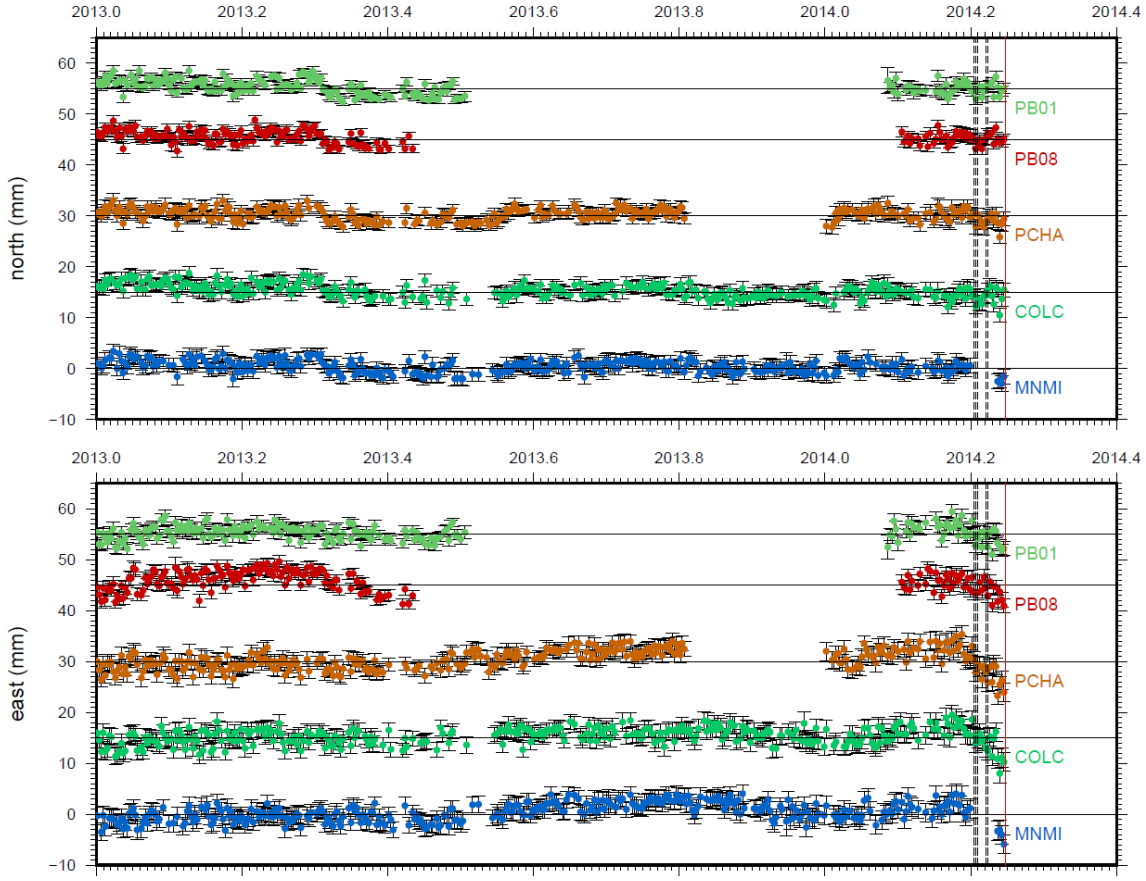

Fig. S12 : Same as Fig.3 in the main text but presenting 2013-2014.4 time-series of permanent GPS stations located inland.

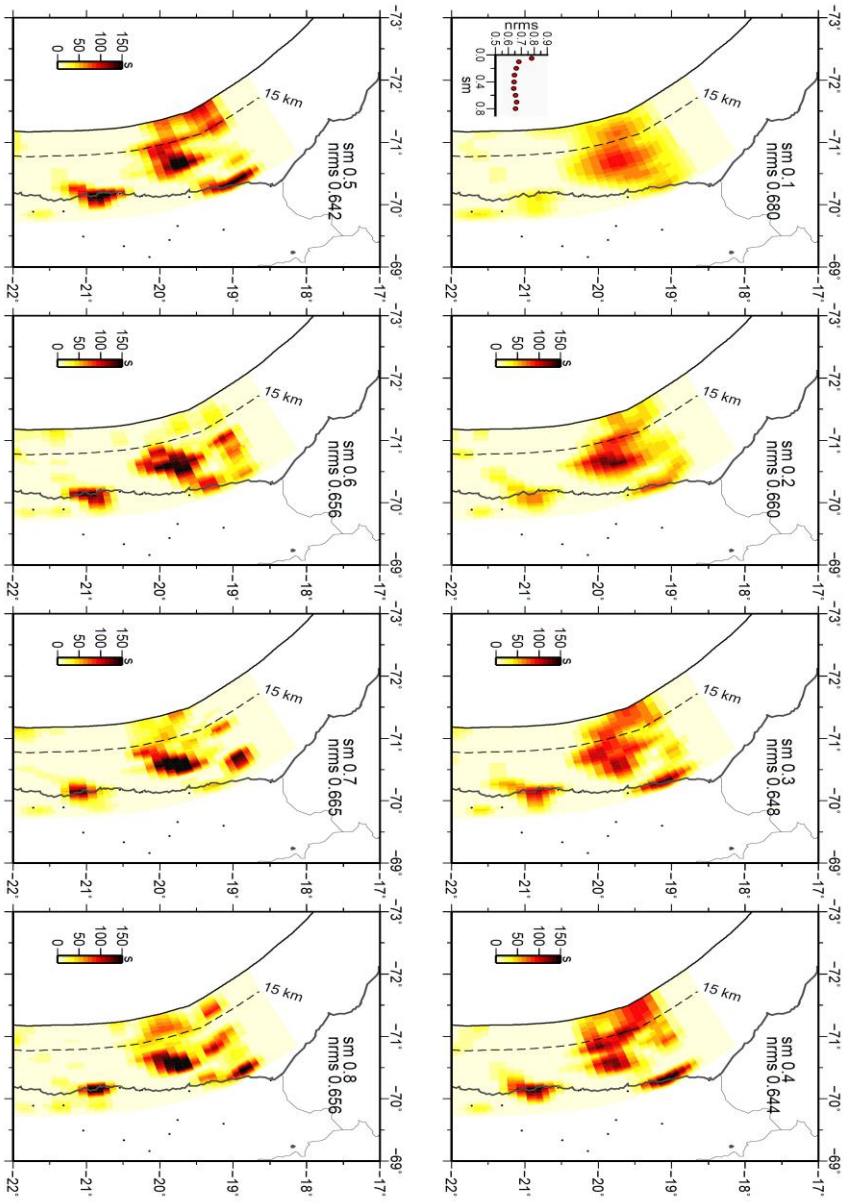

Fig. S13 : Slip patterns (in mm) corresponding to the cumulated motion from 15 to 31 March inverted using different smoothing values. Slip is color coded as in main-text Figure 4. The smoothing value and the normalized root mean square relative to the data are indicated in the upper right corner of each plot.

Table S1 Swarms were defined following the methodology proposed by *(31)* appropriately adapted for Chile *(32)*, using the catalogue published by the Nation Seismological Center of Chile (CSN).

Lat	Long	Depth (km)	M_L	Year	Month	Day
-19.577	-70.780	37.5	4.4	2008	7	9
-19.566	-70.809	40.7	4.0	2008	7	9
-19.591	-70.802	33.2	3.7	2008	7	9
-19.579	-70.812	34.0	4.1	2008	7	9
-18.315	-70.768	38.8	6.5	2010	5	6
-18.300	-70.797	40.3	4.3	2010	5	6
-18.390	-70.724	40.2	4.1	2010	5	6
-19.952	-70.559	38.7	4.0	2010	12	1
-19.946	-70.571	36.2	2.6	2010	12	1
-20.221	-70.810	28.7	3.7	2011	3	23
-20.194	-70.817	26.5	3.9	2011	3	23
-19.671	-70.886	47.7	3.5	2011	4	25
-19.637	-70.879	45.6	2.8	2011	4	25
-19.618	-70.700	40.1	3.3	2011	9	23
-19.648	-70.704	41.1	2.5	2011	9	24
-19.611	-70.687	36.9	3.8	2011	10	1
-19.596	-70.756	40.1	4.6	2011	10	3
-19.588	-70.724	37.9	2.3	2011	10	3
-19.597	-70.773	39.4	2.8	2011	10	3
-19.599	-70.755	36.8	2.4	2011	10	3
-19.590	-70.736	36.1	2.0	2011	10	3
-19.587	-70.762	37.4	2.8	2011	10	3
-19.998	-70.558	22.9	2.7	2012	1	25
-19.995	-70.568	24.9	3.8	2012	1	26
-20.000	-70.556	18.3	2.9	2012	2	12
-19.995	-70.560	23.1	2.9	2012	2	12
-19.618	-70.784	34.2	4.3	2012	2	13
-19.596	-70.752	35.4	3.4	2012	2	13
-19.607	-70.774	35.2	3.8	2012	2	14
-20.077	-70.691	29.7	3.8	2012	5	6
-20.080	-70.684	30.8	3.0	2012	5	6

-20.203	-70.962	27.6	3.1	2012	5	22
-20.182	-70.930	28.0	3.2	2012	5	22
-20.034	-70.568	24.8	2.6	2012	10	1
-20.037	-70.605	23.6	2.5	2012	10	1
-18.504	-71.002	34.4	2.8	2012	11	1
-18.527	-71.002	32.0	3.0	2012	11	2
-20.220	-70.927	38.0	4.9	2013	7	23
-20.227	-70.911	37.1	4.5	2013	7	23
-20.232	-70.875	39.0	4.6	2013	7	23
-20.222	-70.822	37.3	2.4	2013	7	23
-20.245	-70.845	36.0	2.8	2013	7	23
-20.243	-70.894	38.5	4.0	2013	7	23
-20.248	-70.780	39.4	2.8	2013	7	24
-20.180	-70.818	40.4	4.7	2013	7	24
-20.118	-70.830	25.4	2.3	2013	8	14
-20.122	-70.861	14.6	3.6	2013	8	15
-20.121	-70.834	30.9	3.3	2013	8	15
-20.133	-70.853	18.0	2.6	2013	8	15
-20.134	-70.807	26.8	2.9	2013	8	15
-20.118	-70.844	33.2	4.4	2013	8	15
-20.119	-70.812	36.3	4.4	2013	8	16
-20.136	-70.825	24.0	2.7	2013	8	16
-19.592	-70.667	38.9	3.1	2013	8	18
-19.572	-70.664	39.6	3.0	2013	8	18
-19.570	-70.678	39.6	2.7	2013	8	18
-20.133	-70.842	28.6	2.3	2013	8	21
-20.818	-69.164	99.3	3.3	2013	8	22
-20.055	-70.824	28.8	2.4	2013	8	29
-20.057	-70.822	27.0	3.2	2013	8	29
-20.637	-70.622	32.9	2.8	2014	1	8
-20.727	-70.595	32.0	3.9	2014	1	8
-20.619	-70.603	33.1	2.7	2014	1	9
-20.754	-70.583	35.6	3.4	2014	1	9
-19.668	-70.925	38.6	4.1	2014	1	21
-19.676	-70.979	40.4	3.5	2014	1	21
-19.681	-70.964	36.4	3.9	2014	1	21
-19.683	-70.974	37.8	4.0	2014	1	21
-19.668	-71.015	37.6	3.0	2014	1	21
-19.781	-70.204	39.5	2.9	2014	1	22
-19.767	-70.211	41.8	3.6	2014	1	22
-19.424	-71.039	33.6	3.9	2014	2	2

-19.422	-71.029	35.5	3.6	2014	2	3
-19.429	-71.032	35.7	4.4	2014	2	3
-19.402	-71.042	30.9	2.6	2014	2	3
-19.406	-71.039	31.2	3.7	2014	2	3
-19.402	-71.057	32.2	3.9	2014	2	4
-19.434	-71.049	35.0	3.9	2014	2	4
-19.394	-71.024	32.4	3.0	2014	2	4
-19.381	-70.998	35.4	3.3	2014	2	5
-19.419	-71.040	34.7	3.3	2014	2	5
-19.395	-71.039	31.1	2.8	2014	2	6
-19.436	-71.034	32.4	3.5	2014	2	16
-19.445	-71.022	36.9	3.8	2014	2	16

Tab. S2 : Table of calculated offsets at permanent GPS stations in North Chile. Cumulated offset from 10 to 31 March 2014 and associated uncertainties are given in columns 4 to 7. Offsets associated to the coseismic motion of 16 March 2014 and associated uncertainties are given in columns 8 to 11 (mm); offsets associated to 10-31 March 2014 slow-slip motion and associated uncertainties are given in columns 12 to 18 (mm).

NAME	Lat	Lon	Cumulated				Coseismic 16 March Mw 6.7				SSE (17 to 31 March)			
			E	N	sE	sN	E	N	sE	sN	E	N	sE	sN
AEDA	289.822	-20.546	-4.57	4.64	3.53	2.92	-2.13	0.82	2.83	2.36	-2.44	3.82	4.24	3.49
MNMI	290.404	-19.131	-7.67	-2.79	1.88	2.14	-	-	-	-	-	-	-	-
COLC	291.361	-19.276	-5.32	-0.01	4.02	3.65	0.35	-1.32	3.29	2.99	-5.67	1.31	4.75	4.32
IQQE	289.868	-20.273	-10.12	1.14	3.7	3.23	-3.82	1.02	3.03	2.64	-6.3	0.12	4.37	3.82
PB01	290.512	-21.044	-4.27	0.45	3.66	3.38	-1.15	-0.33	3	2.76	-3.12	0.78	4.32	4
PB02	290.107	-21.315	-3.45	0.51	3.87	3.3	-0.18	0.09	3.17	2.7	-3.27	0.42	4.57	3.9
PB03	290.248	-22.049	-1.76	-0.47	4.19	3.47	-0.57	0.26	3.45	2.85	-1.19	-0.73	4.94	4.09
PB04	289.850	-22.335	-1.64	0.5	3.85	3.4	-0.12	0.21	3.15	2.78	-1.52	0.29	4.54	4.01
PB07	290.114	-21.727	-1.84	-0.37	3.91	3.36	-0.43	0.39	3.21	2.75	-1.41	-0.76	4.6	3.96
PB08	290.839	-20.143	-5.46	0.02	3.97	3.45	0.33	-0.82	3.26	2.83	-5.79	0.84	4.68	4.08
PB11	290.344	-19.761	-6.69	1.54	3.39	2.88	-1.37	-0.57	2.75	2.33	-5.32	2.11	4.02	3.42
PCHA	290.568	-19.869	-6.61	-1.56	3.72	3.47	-1.55	-0.87	3.04	2.84	-5.06	-0.69	4.4	4.1
PICC	290.665	-20.490	-4.27	0.2	3.92	3.56	-0.45	0.12	3.2	2.9	-3.82	0.08	4.63	4.23
PSGA	289.877	-19.597	-18.01	-6.56	3.73	3.25	-2.06	-3.07	3.04	2.64	-15.95	-3.49	4.42	3.85
UAPE	289.859	-20.243	-8.09	2.11	4.72	3.96	-5.13	0.2	3.81	3.21	-2.96	1.91	5.63	4.72
UTAR	289.704	-18.491	-5.25	-2.28	4.28	3.9	0.64	-1.71	3,49	3.17	-5.89	-0.57	5.07	4.63

References and Notes

1. F. Montessus de Ballore, *Historia Sísmica de los Andes Meridionales*, 6 vols. (Editorial Cervantes, Santiago de Chile, 1916).

2. E. Kausel, *Bol. Acad. Chil. Ciencias* **3**, 8–12 (1986).

3. C. Lomnitz, *Geofis. Panamericana* **1**, 151–178 (1971).

4. D. Comte, M. Pardo, Reappraisal of great historical earthquakes in the northern Chile and southern Peru seismic gaps. *Nat. Hazards* **4**, 23–44 (1991). doi:10.1007/BF00126557

5. M. Metois, A. Socquet, C. Vigny, D. Carrizo, S. Peyrat, A. Delorme, E. Maureira, M.-C. Valderas-Bermejo, I. Ortega, Revisiting the North Chile seismic gap segmentation using GPS-derived interseismic coupling. *Geophys. J. Int.* **194**, 1283–1294 (2013). doi:10.1093/gji/ggt183

6. M. Malgrange, R. Madariaga, Complex distribution of large thrust and normal fault earthquakes in the Chilean subduction zone. *Geophys. J. R. Astron. Soc.* **73**, 489–505 (1983). doi:10.1111/j.1365-246X.1983.tb03326.x

7. S. Peyrat, R. Madariaga, E. Buforn, J. Campos, G. Asch, J. P. Vilotte, Kinematic rupture process of the 2007 Tocopilla earthquake and its main aftershocks from teleseismic and strong-motion data. *Geophys. J. Int.* **182**, 1411–1430 (2010). doi:10.1111/j.1365-246X.2010.04685.x

8. A. Fuenzalida, B. Schurr, M. Lancieri, M. Sobiesiak, R. Madariaga, High-resolution relocation and mechanism of aftershocks of the 2007 Tocopilla (Chile) earthquake. *Geophys. J. Int.* **194**, 1216–1238 (2013). doi:10.1093/gji/ggt163

9. E. R. Engdahl, A. Villaseñor, in *International Handbook of Earthquake and Engineering Seismology*, Part A, Ch. 41 (Academic Press, 2002).

10. M. Chlieh, H. Perfettini, H. Tavera, J.-P. Avouac, D. Remy, J.-M. Nocquet, F. Rolandone, F. Bondoux, G. Gabalda, S. Bonvalot, Interseismic coupling and seismic potential along the Central Andes subduction zone. *J. Geophys. Res.* **116**, B12405 (2011). doi:10.1029/2010JB008166

11. M. Béjar-Pizarro, A. Socquet, R. Armijo, D. Carrizo, J. Genrich, M. Simons, Andean structural control on interseismic coupling in the North Chile subduction zone. *Nat. Geosci.* **6**, 462–467 (2013). doi:10.1038/ngeo1802

12. Th. Lay, H. Yue, E. Brodsky, C. An, The 1 April 2014 Iquique, Chile, M_w 8.1 earthquake rupture sequence. *Geophys. Res. Lett.* **41**, 3818–3825 (2014). doi:10.1002/2014GL060238

13. Y. Yagi, R. Okuwaki, B. Enescu, S. Hirano, Y. Yamagami, S. Endo, T. Komoro, Rupture process of the 2014 Iquique Chile earthquake in relation with the foreshock activity. *Geophys. Res. Lett.* **41**, 4201–4206 (2014).

14. Information on materials and methods is available on *Science* Online.

15. M. E. Pasyanos, D. S. Dreger, B. Romanowicz, *Bull. Seismol. Soc. Am.* **86**, 1255–1269 (1996).

16. G. Hayes, D. J. Wald, R. L. Johnson, Slab1.0: A three-dimensional model of global subduction zone geometries. *J. Geophys. Res.* **117**, B01302 (2012). doi:10.1029/2011JB008524

17. M. Kikuchi, H. Kanamori, *Bull. Seismol. Soc. Am.* **81**, 2335–2350 (1991).

18. S. Ozawa, H. Saito, M. Tobita, *Earth Planets Space* **59**, 1241–1245 (2007).

19. W. L. Ellsworth, G. C. Beroza, Seismic evidence for an earthquake nucleation phase. *Science* **268**, 851–855 (1995). Medline doi:10.1126/science.268.5212.851

20. S. Latour, A. Schubnel, S. Nielsen, R. Madariaga, S. Vinciguerra, Characterization of nucleation during laboratory earthquakes. *Geophys. Res. Lett.* **40**, 5064–5069 (2013). doi:10.1002/grl.50974

21. E. Contreras-Reyes, J. Jara, I. Grevemayer, S. Ruiz, D. Carrizo, Abrupt change in the dip of the subducting plate beneath north Chile. *Nat. Geosci.* **5**, 342–345 (2012). doi:10.1038/ngeo1447

22. D. Comte, A. Eisenberg, E. Lorca, M. Pardo, L. Ponce, R. Saragoni, S. K. Singh, G. Suárez, The 1985 central chile earthquake: A repeat of previous great earthquakes in the region? *Science* **233**, 449–453 (1986). Medline doi:10.1126/science.233.4762.449

23. R. Madariaga, M. Métois, C. Vigny, J. Campos, Central Chile finally breaks. *Science* **328**, 181–182 (2010). Medline doi:10.1126/science.1189197

24. A. Kato, K. Obara, T. Igarashi, H. Tsuruoka, S. Nakagawa, N. Hirata, Propagation of slow slip leading up to the 2011 M_w 9.0 Tohoku-Oki earthquake. *Science* **335**, 705–708 (2012). Medline doi:10.1126/science.1215141

25. J. C. Ruegg, M. Olcay, D. Lazo, Co-, post- and pre(?)-seismic displacements associated with the Mw 8.4 southern Peru earthquake of 23 June 2001 from continuous GPS measurements. *Seismol. Res. Lett.* **72**, 673–678 (2001). doi:10.1785/gssrl.72.6.673

26. A. Lomax, J. Virieux, P. Volant, C. Berge, in *Advances in Seismic Event Location*, (Kluwer, Amsterdam, 2000), pp. 101–134.

27. S. Husen, E. Kissling, E. Flueh, Local earthquake tomography of shallow subduction in north Chile: A combined onshore and offshore study. *J. Geophys. Res.* **105**, 28183–28198 (2000). doi:10.1029/2000JB900229

28. Z. Altamimi, X. Collilieux, L. Métivier, ITRF2008: An improved solution of the international terrestrial reference frame. *J. Geod.* **85**, 457–473 (2011). doi:10.1007/s00190-011-0444-4

29. R. McCaffrey, in *Plate Boundary Zones*, S. Stein, J. Freymueller, Eds., (AGU Geodynamics Series 30, 2002), pp. 101–122.

30. K. Chanard, J. P. Avouac, G. Ramillien, J. Genrich, Modeling deformation induced by seasonal variations of continental water in the Himalaya region: Sensitivity to Earth elastic structure. *J. Geophys. Res.* **119**, 5097–5113 (2014).

31. P. Reasenberg, Second-order moment of central California seismicity, 1969–1982. *J. Geophys. Res.* **90**, 5479–5495 (1985). doi:10.1029/JB090iB07p05479

32. F. Leyton, S. Ruiz, S. A. Sepúlveda, Preliminary re-evaluation of probabilistic seismic hazard assessment in Chile: From Arica to Taitao Peninsula. *Adv. Geosci.* **22**, 147–153 (2009). doi:10.5194/adgeo-22-147-2009